JVST B
Journal of Vacuum Science & Technology B

Diffusion of implanted Ge and Sn in β-Ga_2O_3

Cite as: J. Vac. Sci. Technol. B **37**, 051204 (2019); https://doi.org/10.1116/1.5118001
Submitted: 02 July 2019 . Accepted: 05 August 2019 . Published Online: 27 August 2019

Ribhu Sharma, Mark E. Law, Minghan Xian, Marko Tadjer, Elaf A. Anber, Daniel Foley, Andrew C. Lang, James L. Hart, James Nathaniel, Mitra L. Taheri, Fan Ren, S. J. Pearton, and A. Kuramata

Diffusion of implanted Ge and Sn in β-Ga_2O_3

Ribhu Sharma,[1] Mark E. Law,[2] Minghan Xian,[3] Marko Tadjer,[4] Elaf A. Anber,[5] Daniel Foley,[5] Andrew C. Lang,[5] James L. Hart,[5] James Nathaniel,[5] Mitra L. Taheri,[5] Fan Ren,[3] S. J. Pearton,[1,a)] and A. Kuramata[6]
[1]*Department of Materials Science and Engineering, University of Florida, Gainesville, Florida 32611*
[2]*Department of Electrical and Computer Engineering, University of Florida, Gainesville, Florida 32611*
[3]*Department of Chemical Engineering, University of Florida, Gainesville, Florida 32611*
[4]*U.S. Naval Research Laboratory, 4555 Overlook Ave. SW, Washington, DC 20375*
[5]*Department of Materials Science and Engineering, Drexel University, Philadelphia, Pennsylvania 19104*
[6]*Tamura Corp. and Novel Crystal Technology, Sayama City, Saitama 350-1328, Japan*

(Received 2 July 2019; accepted 5 August 2019; published 27 August 2019)

The n-type dopants, Ge and Sn, were implanted into bulk (−201) β-Ga_2O_3 at multiple energies (60, 100, 200 keV) and total doses of ~10^{14} cm^{-2} and annealed at 1100 °C for 10–120 s under either O_2 or N_2 ambients. The Ge-implanted samples showed almost complete recovery of the initial damage band under these conditions, with the disordered region decreasing from 130 to 17 nm after 1100 °C anneals. Fitting of secondary ion mass spectrometry profiles was used to obtain the diffusivity of both Ge and Sn, with values at 1100 °C of 1.05×10^{-11} $cm\,s^{-1}$ for Ge and 2.7×10^{-13} $cm\,s^{-1}$ for Sn for annealing under O_2 ambients. Some of the dopant is lost to the surface during these anneals, with a surface outgas rate of $1–3 \times 10^{-7}$ s^{-1}. By sharp contrast, the redistribution of both dopants was almost completely suppressed during annealing in N_2 ambients under the same conditions, showing the strong influence of point defects on dopant diffusivity of these implanted dopants in β-Ga_2O_3. *Published by the AVS.* https://doi.org/10.1116/1.5118001

I. INTRODUCTION

N-type doping of β-Ga_2O_3 during crystal growth is typically performed with the tetravalent ions Si, Sn, and Ge, which have hydrogenic shallow donor states (ionization levels in the range of 10–30 meV).[1–7] It has been noted that high temperature annealing of undoped and Sn-doped bulk crystals can have significant effects on the resulting conductivity, especially in O_2 ambients, where the material may become insulating.[6,8–11] The initial work on β-Ga_2O_3 found that unintentionally doped samples showed increasing charge carrier concentrations upon annealing in reducing atmospheres,[2,5] suggesting that oxygen vacancies were the dominant donors present. However, it is now known that oxygen vacancies are deep donors and do not contribute significantly to the n-type conduction,[12] which is now attributed to impurities like Si.[5] Similarly, the active fraction of Si is <50% in bulk crystals, indicating that not all are occupying substitutional Ga sites, although there are two Ga sites in the Ga_2O_3 lattice, and it is expected that the ionization level is lower for the Ga(I) site compared to the octahedral Ga(II) site.[13,14] Ge and Sn are often preferred as dopants, especially in molecular beam epitaxy, because of reduced problems with oxidation of the dopant sources relative to Si.[15–17] Finally, Ge should be an ideal fit for Ga substitution, based on their similar sizes and, therefore, potentially be an efficient donor impurity.

There is increasing interest in doping Ga_2O_3 using ion implantation.[18–26] This provides a versatile method for doping selective area channel and contact regions in field effect transistors.[18,19] Implantation can also be used to create resistive, current-defining paths by incorporating deep acceptors like Fe, Mg_{Ga}, and N_O.[20–24] Peelaers *et al.*[27] examined the diffusion mechanisms for Mg and N and found that diffusion of N was predominantly assisted by O vacancies, while Mg diffusion was controlled by the gallium interstitial concentration. Tadjer *et al.*[26] reported diffusivities at 1150 °C of 9.5×10^{-13} $cm^2\,s^{-1}$ for implanted Si and 1.7×10^{-13} $cm^2\,s^{-1}$ for Sn when annealed under O_2. Sharma *et al.*[28] noted a strong dependence of diffusivity of implanted Si on whether N_2 or O_2 annealing ambients were used, emphasizing the role of defects in assisting implanted dopant migration. Wong *et al.*[29] also noted that implantation damage enhanced the diffusivity of Fe in adjoining layers as a result of defect migration during annealing. There is clearly a need to more fully understand the diffusion of implanted dopants in Ga_2O_3 if this approach is to be used in a controlled fashion during device fabrication.

In this paper, unintentionally doped, edge-defined, film-fed (EFG)-grown (−201) β-Ga_2O_3 substrates were implanted with Ge or Sn ions with multiple energies in the 60–200 keV range in order to obtain a peak concentration of both dopants of ~10^{19} cm^{-3}. The samples were then annealed at 1100 °C for various times (10–120 s) under O_2 or N_2 ambients to repair the ion damage and activate the donors onto substitutional lattice sites. The samples were characterized by secondary ion mass spectrometry (SIMS) and cross-sectional transmission electron microscopy (TEM) before and after annealing. Both dopants were found to exhibit significant diffusivity for annealing under O_2 ambient, but this was suppressed in N_2 ambients.

II. EXPERIMENT

The samples were obtained from Novel Crystal Technology[6] and were unintentionally doped EFG Ga_2O_3 substrates (no epi), with a room temperature carrier concentration

a)Electronic mail: spear@mse.ufl.edu

of $1–2 \times 10^{17}\,cm^{-3}$, as measured by the electrochemical capacitance-voltage method. They had (−201) orientation, with XRD FWHM rocking curves of 20 arcsec and 25 arcsec in the [010] and [102] directions, respectively.

All samples were implanted nominally at room temperature with a 7° tilt with respect to the beam normal. Ge and Sn ions at multiple energies and doses were employed to obtain near-uniform concentrations of $10^{19}\,cm^{-3}$. The specific energy and dose conditions were $2 \times 10^{13}\,cm^{-2}$/60 keV + $3 \times 10^{13}\,cm^{-2}$/100 keV + $4 \times 10^{13}\,cm^{-2}$/200 keV for Sn and $3 \times 10^{13}\,cm^{-2}$/60 keV + $5 \times 10^{13}\,cm^{-2}$/100 keV + $7 \times 10^{13}\,cm^{-2}$/200 keV for Ge.

The samples were annealed in 1 atm of pure, flowing N_2 or O_2 at 1100 °C for various times (10–120 s) in a Surface Science Integration (SSI) Solaris 150 rapid thermal anneal system. Microstructural analysis was carried out on Ge-implanted and annealed samples using Scanning TEM (STEM) mode on a JEOL 2100 field emission TEM, equipped with a high-resolution pole piece. SIMS was performed at Evans Analytical with a magnetic sector Cameca system using a Cs^+ ion beam with 14.5 keV energy and 24° incident angle. The SIMS profiles were fitted using the FLorida Object Oriented Device Process Simulator (FLOOPS) via a Fick diffusion-based model.[30,31]

III. RESULTS AND DISCUSSION

Figure 1 shows STEM high-angle annular dark-field (HAADF) results, with an isolated band of damage after Ge implantation, which extends ~130 nm (left) from the sample surface and corresponds to the projected range of Ge under these energy conditions. The end-of-range damage region in this as-implanted sample consists of extended defects created by the nuclear collision energy loss during the ion stopping process. After annealing at 1100 °C for 10 s under O_2, STEM imaging shows that implantation-induced damage is almost fully recovered, with the damage band decreased to ~17 nm from the sample surface.

We observed extensive redistribution of both the Ge and Sn during annealing in O_2. Figure 2 shows the experimental (a) and the fits to the annealed profiles (b) for Sn. There is both diffusion into the bulk and loss of dopant to the surface. The model used within FLOOPS is based on Fickian diffusion, the influence of vacancies and interstitials, and the trapping and release of the dopant atoms on damage sites created by the implantation and included segregation to the surface, represented by

$$\left(\frac{dV}{dt} - D_V \frac{d}{dx}\frac{dV}{dx} + R + K_{DA}\,(V - E_V)(I - E_V)\right) = 0,$$

$$\left(\frac{dI}{dt} - D_I \frac{d}{dx}\frac{dI}{dx} + K_{DA}(V - E_V)(I - E_V)\right) = 0,$$

$$K_s \cdot Sn = 0,$$

where K_s is the rate of loss to the surface of the diffusing species, D_V and D_I are the vacancy and interstitial diffusion,

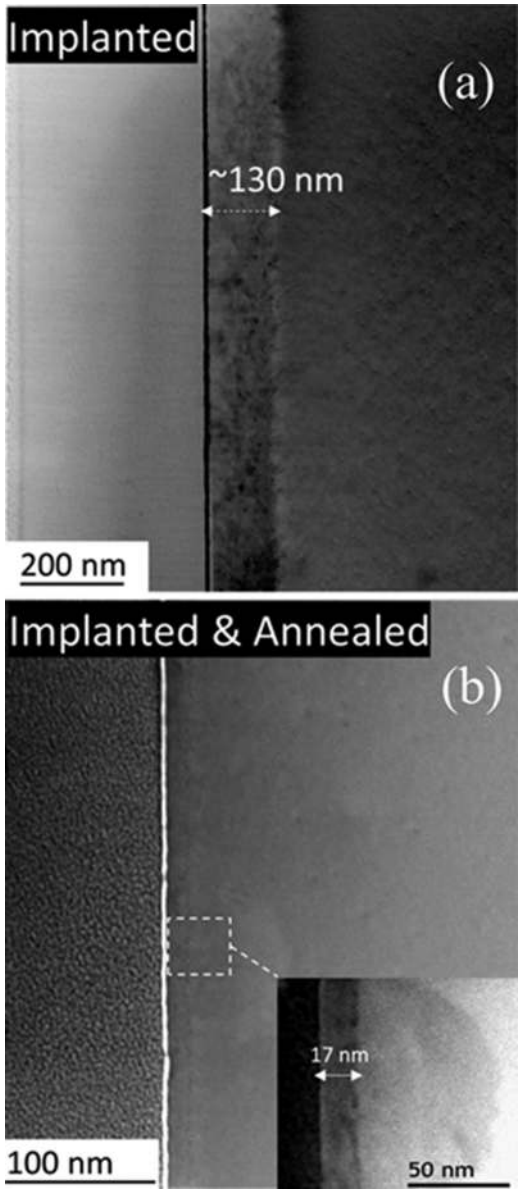

FIG. 1. Cross-sectional STEM/HADAAF image of Ge-implanted Ga_2O_3, showing the presence of isolated band of damage after implantation (a) and STEM-HADAAF image of implanted-annealed sample (b) where only ~17 nm of the damage zone remains.

respectively, K_{DA} is the rate of damage annealing, I is the interstitial concentration, and E_V is the equilibrium damage concentration (assumed to be $10^{15}\,cm^{-3}$).[32,33]

We have used a similar model previously for diffusion of deuterium in Ga_2O_3.[34] The rate of change of the mobile Sn concentration is represented by

$$\frac{dSn}{dt} - D_{Sn}\frac{d}{dx}\frac{dSn}{dx} + R = 0,$$

where D_{Sn} is the Sn diffusivity, Sn is the Sn concentration, and R is the reaction rate representing the trapping on damage sites given by

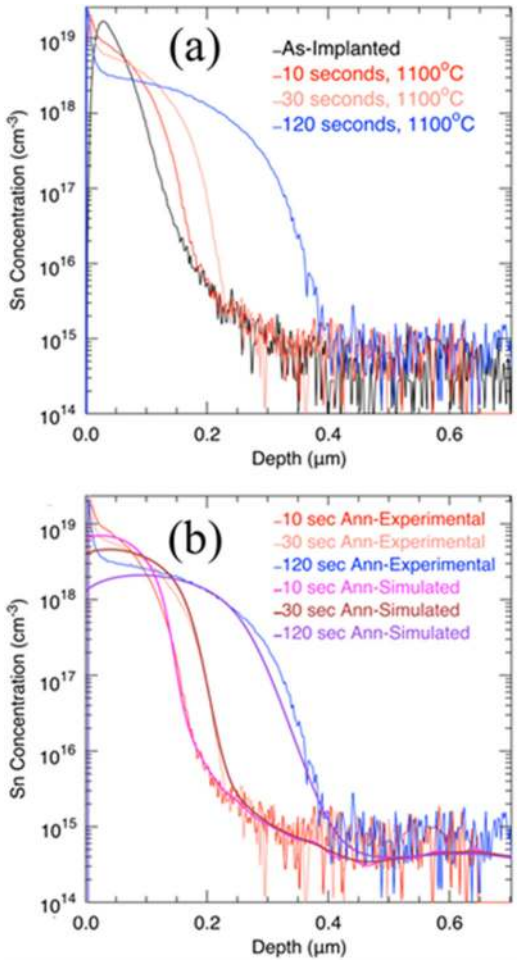

FIG. 2. Experimental (a) and simulated fits (b) of the SIMS profiles of Sn implanted in Ga_2O_3 and subsequently annealed for different times at 1100 °C in O_2 ambient.

$$R = (K_T \cdot Sn \cdot V) - (K_R \cdot T).$$

We achieved accurate fits for the Sn profiles assuming a diffusivity of 2.7×10^{-13} cm s^{-1} at 1100 °C under O_2. The other fitting parameters are summarized in Table I, with a vacancy diffusion rate of 10^{-8} cm s^{-1}, trap rate on damage sites of 8×10^{-16} s^{-1}, and a release rate of 1.2 s^{-1}. The difference between the ion-implanted preanneal damage concentration and trapped Sn concentration is considered the equilibrium vacancy concentration and was obtained from the incorporation of stopping and range of ions in matter[35] data.

TABLE I. Summary of fitting parameters obtained from FLOOPS for annealing of both dopants in O_2 ambients.

Parameters/rates	Sn	Ge
Diffusivity (cm^2 s^{-1})	2.7×10^{-13}	1.1×10^{-11}
Trap rate on damage sites (s^{-1})	8.0×10^{-16}	8.0×10^{-16}
Release rate (s^{-1})	1.2	1
Vacancy diffusivity (cm^2 s^{-1})	2.0×10^{-8}	7.0×10^{-8}
Surface outgas rate (s^{-1})	1.3×10^{-7}	7.0×10^{-7}

The huge contrast for the results obtained with annealing of Sn implants in a N_2 ambient is shown in Fig. 3(a) for the case of annealing at 1100 °C for 120 s. The figure shows the simulated fit to the experimental Sn profiles for annealing in N_2, as well as the total concentration of vacancies after annealing. The total vacancy concentration for annealing in N_2 is higher than for O_2 annealing, according to the simulations involving a vacancy inflow and outflow from the surface and an example is shown in Fig. 3(b).

We observed similar suppression of the diffusion when annealing in N_2 for implanted Si previously.[28] This emphasizes the effect of the point defect population present in the near-surface region on the diffusion of the implanted dopants. Since the mobile Sn is experimentally observed to be trapped at vacancies for N_2 anneals, they are likely Ga_v. Use of the N_2 annealing ambient should supply more O_v, but these have a very high migration energy[36] so that Ga_v control the site occupation and the reduced migration of the Sn.[35] Both O_v and Ga_v have very complex migration paths in monoclinic Ga_2O_3.[36] More work is needed to establish the charge state of the O_v (neutral or 2+) or Ga_v (neutral, 1−, 2−, or 3−)[37–39]

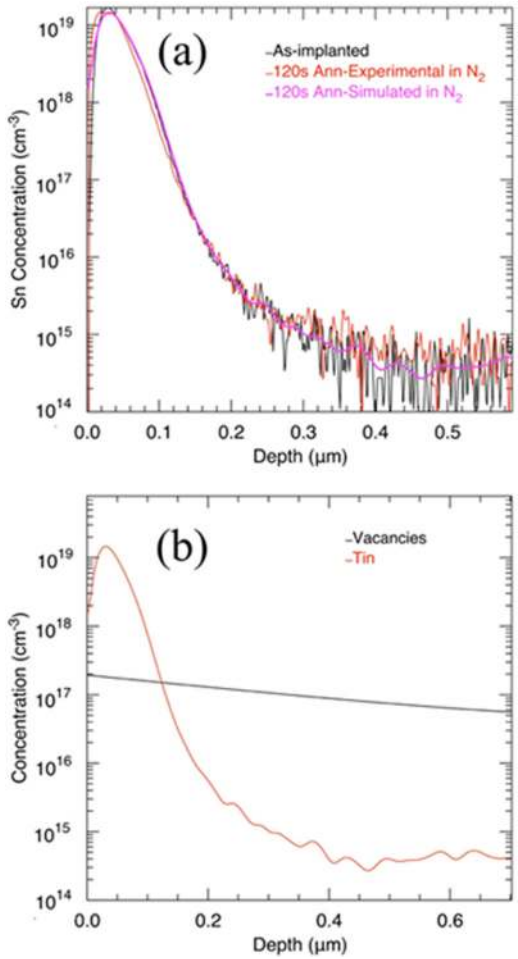

FIG. 3. Experimental and simulated fits of the SIMS profile (a) and simulated vacancy and total Sn (trapped plus mobile Sn) concentrations (b) in Sn-implanted Ga_2O_3 after annealing in N_2 ambient at 1100 °C for 120 s.

that control the migration and site occupation of the Sn. However, work by Korhonen *et al.*[40] using positron annihilation spectroscopy established that O_2 annealing led to an increase in Ga_v density. Similarly, it has been determined that Sn preferentially occupies the Ga(2) octahedral site,[41] and hence it is likely that Ga_v can enhance the diffusivity of these substitutional species.

Similar results and trends were found for the implanted Ge. Figure 4 shows the experimental (a) and the fits to the annealed profiles (b) for Ge after annealing in O_2 for different times. The redistribution is even more pronounced than for Sn, as evidenced by the higher diffusivity of 1.1×10^{-11} cm s^{-1} at 1100 °C. While Ge is a smaller atom than Sn and might be expected to diffuse faster, we note that the diffusivity is even faster than for Si under the same conditions (4.5×10^{-12} cms^{-1}), so that size is not the only determining factor.

The suppression of diffusion for Ge in N_2 annealing ambients is shown in Fig. 5(a). The fit to the experimental data is not as accurate in this case, which may be due to a more pronounced concentration dependence of the diffusivity in the case of Ge. There is a higher concentration of vacancies present according to the simulations [Fig. 5(b)], and this may cause compensation on the end-of-range region of the profile. At this stage, we have not performed electrical profiling experiments to confirm this, since the control of impurities and defects in the starting material needs optimization and spatial measurements of activation would likely not be reproducible.

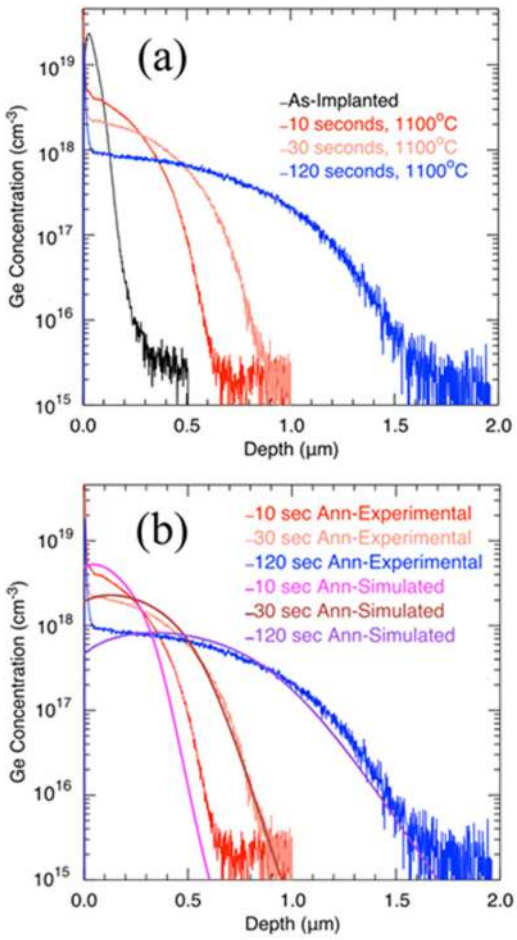

FIG. 4. Experimental (a) and simulated fits (b) of SIMS profiles of Ge implanted in Ga_2O_3 and subsequently annealed for different times at 1100 °C in O_2 ambient.

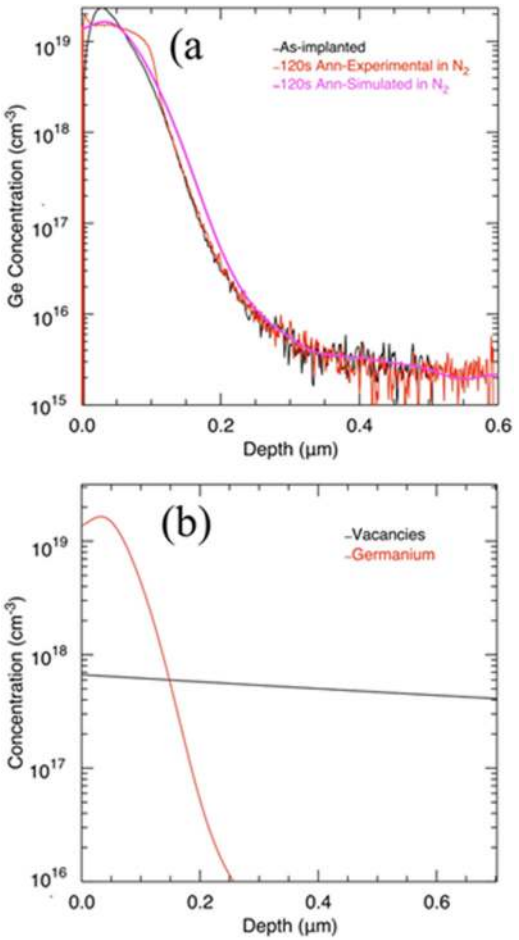

FIG. 5. Experimental and simulated fits of the SIMS profile (a) and simulated vacancy and total Ge (trapped plus mobile Ge) concentrations (b) in Ge-implanted Ga_2O_3 after annealing in N_2 ambient at 1100 °C for 120 s.

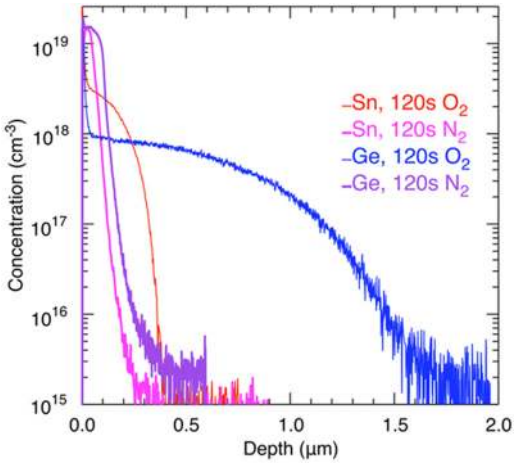

FIG. 6. Comparison of Sn and Ge ion profiles after annealing at 1100 °C for 120 s in either O_2 or N_2 ambients.

To give a direct comparison of the redistribution of Sn versus Ge under the same conditions, Fig. 6 shows the SIMS profiles for annealing at 1100 °C for 120 s in either O_2 orN_2 ambients. These data clearly show the effect of the ambient and the more rapid diffusion of Ge relative to Sn. It will be interesting in future experiments to independently control the amount of lattice damage by using an inert species like Ar to provide a controlled damage density that can be varied relative to the intrinsic damage from the Sn or Ge implants themselves. This may help elucidate whether the additional vacancy concentration created by the heavier Sn is the dominant factor in determining its subsequent redistribution. It will also be of interest to see if Ge is a faster diffuser in doped epitaxial layers, where there is an absence of implant damage.

IV. SUMMARY AND CONCLUSIONS

We have observed a dramatic effect of annealing ambient on the diffusivity of implanted Sn and Ge in β-Ga_2O_3. Both of those donor dopants exhibit significant redistribution during annealing in O_2 ambients, whereas this motion is suppressed for N_2 annealing ambients. The experimental profiles can be accurately fit with a model involving Fickian diffusion of mobile Sn or Ge, with trapping at vacancies and loss to the surface. This model currently cannot differentiate between Ga and O vacancies in determining the diffusion enhancement, but since both Sn and Ge occupy Ga substitutional sites, we can assume that Ga_v are the controlling factor during N_2 annealing since the dopants are less mobile and are trapped at these vacancies.

ACKNOWLEDGMENTS

The work at the UF was sponsored by the Department of the Defense, Defense Threat Reduction Agency (No. HDTRA1-17-1-011), monitored by Jacob Calkins and also by the NSF DMR (No. 1856662, Tania Paskova). Research at the NRL was supported by the Office of Naval Research (ONR). Research at Drexel was supported from the NSF MRI (Award No. 1429661). Research at Novel Crystal Technology was partially supported by ONR Global (Grant No. N62909-16-1-2217).

[1]K. Irmscher, Z. Galazka, M. Pietsch, R. Uecker, and R. Fornari, J. Appl. Phys. **110**, 063720 (2011).
[2]H. von Wenckstern, Adv. Electron. Mater. **3**, 1600350 (2017).
[3]M. Higashiwaki, K. Sasaki, H. Murakami, Y. Kumagai, A. Koukitu, and A. Kuramata, Semicond. Sci. Technol. **31**, 034001 (2016).
[4]S. J. Pearton, J. Yang, P. H. Cary, F. Ren, J. Kim, M. J. Tadjer, and Michael A. Mastro, Appl. Phys. Rev. **5**, 011301 (2018).
[5]Zbigniew Galazka, Semicond. Sci. Technol. **33**, 113001 (2018).
[6]A. Kuramata, K. Koshi, S. Watanabe, Y. Yamaoka, T. Masui, and S. Yamakoshi, Jpn. J. Appl. Phys. **55**, 1202A2 (2016).
[7]Adam T. Neal *et al.*, Appl. Phys. Lett. **113**, 062101 (2018).
[8]N. Ueda, H. Hosono, R. Waseda, and H. Kawazoe, Appl. Phys. Lett. **70**, 3561 (1997).
[9]E. G. Villora, Y. Morioka, T. Atou, T. Sugawara, M. Kikuchi, and T. Fukuda, Phys. Status Solidi A **193**, 187 (2002).
[10]E. G. Villora, K. Hatanaka, H. Odaka, T. Sugawara, T. Miura, H. Fukumura, and T. Fukuda, Solid State Commun. **127**, 385 (2003).
[11]Marko J. Tadjer *et al.*, Proc. SPIE **10532**, 1053212 (2018).
[12]J. B. Varley, J. R. Weber, A. Janotti, and C. G. Van de Walle, Appl. Phys. Lett. **97**, 142106 (2010).
[13]A. T. Neal, S. Mou, R. Lopez, J. V. Li, D. B. Thomson, K. D. Chabak, and G. H. Jessen, Sci. Rep. **7**, 13218 (2017).
[14]K. Iwaya, R. Shimizu, H. Aida, T. Hashizume, and T. Hitosugi, Appl. Phys. Lett. **98**, 142116 (2011).
[15]K. Sasaki, M. Higashiwaki, A. Kuramata, T. Masui, and S. Yamakoshi, J. Cryst. Growth **392**, 30 (2014).
[16]E. Ahmadi, O. S. Koksaldi, S. W. Kaun, Y. Oshima, D. B. Short, U. K. Mishra, and J. S. Speck, Appl. Phys. Express **10**, 041102 (2017).
[17]S.-H. Han, A. Mauze, E. Ahmadi, T. Mates, Y. Oshima, and J. S. Speck, Semicond. Sci. Technol. **33**, 045001 (2018).
[18]K. Sasaki, M. Higashiwaki, A. Kuramata, T. Masui, and S. Yamakoshi, Appl. Phys. Express **6**, 086502 (2013).
[19]M. H. Wong, Y. Nakata, A. Kuramata, S. Yamakoshi, and M. Higashiwaki, Appl. Phys. Express **10**, 041101 (2017).
[20]M. H. Wong, C.-H. Lin, A. Kuramata, S. Yamakoshi, H. Murakami, Y. Kumagai, and M. Higashiwaki, Appl. Phys. Lett. **113**, 102103 (2018).
[21]Marko J. Tadjer, Andrew D. Koehler, Jaime A. Freitas, James C. Gallagher, Matty C. Specht, Evan R. Glaser, Karl D. Hobart, Travis J. Anderson, and Fritz J. Kub, Appl. Phys. Lett. **113**, 192102 (2018).
[22]T. Onuma, Y. Nakata, K. Sasaki, T. Masui, T. Yamaguchi, T. Honda, A. Kuramata, S. Yamakoshi, and M. Higashiwaki, J. Appl. Phys. **124**, 075103 (2018).
[23]Kornelius Tetzner, Andreas Thies, Eldad Bahat Treidel, Frank Brunner, Günter Wagner, and Joachim Würfl, Appl. Phys. Lett. **113**, 172104 (2018).
[24]M. H. Wong, K. Goto, Y. Morikawa, A. Kuramata, S. Yamakoshi, H. Murakami, Y. Kumagai, and M. Higashiwaki, Appl. Phys. Express **11**, 064102 (2018).
[25]Man Hoi Wong, Chia-Hung Lin, Akito Kuramata, Shigenobu Yamakoshi, Hisashi Murakami, Yoshinao Kumagai, and Masataka Higashiwaki, Appl. Phys. Lett. **113**, 102103 (2018).
[26]Marko J. Tadjer *et al.*, ECS J. Solid State Sci. Technol. **8**, Q3133 (2019).
[27]Hartwin Peelaers, John L. Lyons, and Joel B. Varley, APL Mater. **7**, 022519 (2019).
[28]Ribhu Sharma, Mark E. Law, Chaker Fares, Marko Tadjer, Fan Ren, A. Kuramata and S. J. Pearton, AIP Adv. **9**, 085111 (2019).
[29]M. H. Wong, K. Sasaki, A. Kuramata, S. Yamakoshi, and M. Higashiwaki, Appl. Phys. Lett. **106**, 032106 (2015).
[30]See: http://www.flooxs.tec.ufl.edu/
[31]Mark E. Law and Stephen M. Cea, Comput. Mater. Sci. **12**, 289 (1998).
[32]Z. Zhang, E. Farzana, A. R. Arehart, and S. A. Ringel, Appl. Phys. Lett. **108**, 052105 (2016).
[33]K. Irmscher, Z. Galazka, M. Peitsch, R. Uecker, and R. Fornari, J. Appl. Phys. **110**, 063720 (2011).
[34]Ribhu Sharma, Erin Patrick, Mark E. Law, Shihyun Ahn, F. Ren, S. J. Pearton, and Akito Kuramata, ECS J. Solid State Sci. Technol. **6**, 794 (2017).
[35]See: http://www.srim.org/SRIM/SRIMINTRO.htm
[36]A. Kyrtsos, M. Matsubara, and E. Bellottto, Phys. Rev. B **95**, 245202 (2017).
[37]H. Peelaers and C. G. Van de Walle, Phys. Status Solidi B **828** (2015).
[38]J. B. Varley, A. Janotti, C. Franchini, and C. G. Van de Walle, Phys. Rev. B **85**, 081109 (2012).
[39]B. E. Kananen, L. E. Halliburton, K. T. Stevens, G. K. Founds, and N. C. Giles, Appl. Phys. Lett. **110**, 202104 (2017).
[40]E. Korhonen, F. Tuomisto, D. Gogova, G. Wagner, M. Baldini, Z. Galazka, R. Schewski, and M. Albrecht, Appl. Phys. Lett. **106**, 242103 (2015).
[41]S. C. Siah *et al.*, Appl. Phys. Lett. **107**, 252103 (2015).